



Synthesis, Biological Evaluation and In Silico Investigation of Novel Functionalized Imidazole-Based KDM6 Inhibitors



CrossMark

Amr M. El-Araby,^a Omar M. Qassem,^a Ezzat A. El-Sawy,^a Eman Zaghlol El-Razaz,^a
Khaled Abouzid,^{a, b} Rabah A.T. Serya^{a, *}

^aDepartment of Pharmaceutical Chemistry, Faculty of Pharmacy, Ain Shams University, Abbassia, Cairo 11566, Egypt

^bDepartment of Organic and Medicinal Chemistry, Faculty of Pharmacy, University of Sadat City, Menoufia 32897, Egypt

Abstract

Epigenetic markers of the cellular genome are major controllers of the transcriptional level of various genes in physiological and pathological states. These markers are written and erased by epigenetic factors which have been recently studied as potential therapeutic targets of various disease states. Histone lysine demethylases (KDMs) are an example of these epigenetic factors. The histone lysine demethylase subfamily number 6 (KDM6) are an understudied group of these enzymes which have been recently connected to cancers and inflammation. In this work, we conducted a rational and computer-aided approach to design and synthesize KDM6 inhibitors. The designed inhibitors are imidazole-based and are functionalized with variable metal-chelating group to be able to chelate the active site ferrous ion. One of the synthesized compounds, compound 6, was able to inhibit KDM6-expressing cancer cell lines by more than 50% (IC₅₀ = 50.4980% and 50.4699% in HeLa and A549 cells respectively). Molecular docking studies suggest that this compound is able to achieve important active site interactions and coordinate the active site metal through a tridentate interaction. Furthermore, a correlation was established between the structural features and calculated LogP (CLogP) of the tested compounds and their activity. These results represent a promising starting point for the future development of novel KDM6 inhibitors with higher potency.

Keywords: KDM6; JMJD3; GSK-J1; Cervical Cancer; Prostate Cancer; NSCLC; Docking.

1. Introduction

Epigenetic mechanisms in pathological and physiological conditions have been an area of rapid development and research in recent years [1]. The term epigenetics generally comprises all factors and mechanisms that are implicated in the regulation of gene transcription. This regulation takes place via a number of epigenetic modifiers which write or erase chemical tags and markers on the surface of histones or the DNA. These tags then signal for transcriptional factors to either increase, decrease or completely halt the expression of a certain gene. This process of gene regulation makes the reversal of transcriptional states possible by reversing the state of the epigenetic marker responsible [2].

The reversible nature of epigenetic markers has put epigenetic factors under question as potential contributors to disease states. Many studies have confirmed the implication of epigenetics in the development, persistence and progression of many diseases such as neurodegenerative disorders,

autoimmune diseases and inflammation, cancers and viral infections [2-5]. This great implication of epigenetic factors in various disease states has rendered them an interesting target for the development of novel therapeutics [6, 7].

An important player in the modelling of the cellular epigenetic map are the class of histone modifiers. These are families of histone-modifying enzymes that either add or remove chemical markers from certain amino acids on histones such as lysine and arginine [8]. This process of epigenetic marker editing leads to either activation or repression of gene transcription depending on the nature and position of the modified residue [8]. One of the most understudied members of epigenetic factors is the subfamily number 6 of histone lysine demethylases (KDM6). This subfamily of histone demethylases removes methyl groups from trimethylated lysine residues on lysine number 27 of histone number 3 (H3K27me3). The removal of this epigenetic marker activates gene expression at target genes [9].

*Corresponding author e-mail: rabah@pharma.asu.edu.eg; (ggggggggggggggggggggg).

Receive Date: 07 August 2020, Revise Date: 28 November 2020, Accept Date: 30 November 2020

DOI: 10.21608/EJCHEM.2020.38209.2790

©2021 National Information and Documentation Center (NIDOC)

The KDM6 subfamily is comprised of three members; KDM6A (UTX), KDM6B (JMJD3) and KDM6C (UTY) [10]. Despite the similarity of the substrate between all three members of the subfamily, their biochemical function is not constant in physiological and pathological environments. In general, this subfamily of enzymes is implicated in embryonic development under normal conditions. On the other hand, aberrant levels of KDM6 enzymes are found in many diseases such as different cancers and inflammatory conditions [11, 12].

The inhibition of KDM6 for therapeutic purposes has prompted medicinal chemists to conduct discovery campaigns in search for inhibitors. The first ever reported selective inhibitor of the KDM6 subfamily was GSK-J1 (figure 1) reported by the company GlaxoSmithKline in 2012 [13]. The ethyl ester prodrug of this compound, has been used to characterize and establish the biochemical role of KDM6 in many disease states [14-16]. Very few research projects were conducted to further investigate the medicinal chemistry space of KDM6 inhibitors and further characterize the structure-activity relationship features of inhibitory agents [17-19].

In this work, we introduce a novel medicinal chemistry design of chemical entities with potential KDM6 inhibitory activities. The new compounds are based on imidazole-based chemical entities that are functionalized with metal chelating moieties. We also explore *in silico* the potential activity and selectivity of the designed compounds towards the KDM6 subfamily. Due to the implication of KDM6 in the development and progression of cancers of the cervix, prostate and the lung, the designed compounds were synthesized and tested for their activity against PC-3 (prostate), HeLa (Cervix) and A549 (Non-Small Cell Lung Cancer) [14-16].

2. Experimental

2.1. Chemistry

2.1.1. Materials and Device

Starting materials and solvents were purchased from Sigma Aldrich, Loba Chemie and used directly without further purification. Follow up of chemical reactions was performed using TLC plates made of fused silica purchased from Merck, type 60 F254; visualized by UV lamp (254 nm). ¹H NMR spectra were determined by a Bruker NMR instrument at 400 MHz in δ scale (ppm) and J value in Hz at Center for Drug Discovery Research and Development, Ain Shams University using (DMSO-d₆) as the solvent. Melting point was detected by Stuart SMP10 apparatus at Faculty of Pharmacy, Ain Shams

University and are uncorrected. HPLC-Mass Spectrometry findings were measured by Agilent 1100 / ZQ MSD including C18 column and diode array UV detector. The analytes were separated using an Macherey-Nagel Nucleodur-C18 column (150 mm length \times 4.6 mm i.d., 5 μ m) (Macherey-Nagel GMBH & Co., KG, Duren, Germany). The mobile phase (containing 0.01 M ammonium acetate) was gradient starting from 20% acetonitrile to 80% acetonitrile. All products were purified by recrystallization from ethanol. Elemental analysis for all the final products was performed at The Regional Centre for Mycology and Biotechnology, Al-Azhar University.

2.1.2. Synthesis

The general steps for synthesis are summarized in scheme 1.

N-Acylglycines B(1-3) were synthesized using a known chemical procedure for formation of amides from the appropriate carboxylic acids (S1,S2,S3) with ethylglycinate HCL to yield the corresponding N-acyl glycines (A1,A2,A3) respectively. This was followed by saponification using LiOH to produce N-Acylglycines (B1,B2,B3) [20].

General Procedure for preparation of oxazolones (C1 - C3)

Prepare a solution of 20 mmols of N-acylglycine (B1,B2,B3) in acetic anhydride. To the same flask, add 1.2 equivalents of NaOAc and 1 equivalent of imidazole-2-carbaldehyde at room temperature. Stir the reaction mixture at 95-135°C until the completion of the reaction, monitored by TLC. Cool the reaction mixture then refrigerate overnight. The mixture is then allowed to thaw at room temperature and filtered. The solid product is a yellow powder which is then washed with saturated solution of NaHCO₃ and filtered then washed again with petroleum ether and filtered. The products were used in further reactions without characterization [21]. (Z)-4-((1H-imidazol-2-yl)methylene)-2-((E)-4-hydroxystyryl)oxazol-5(4H)-one (C1); yield 79%, (Z)-4-((1H-imidazol-2-yl)methylene)-2-([1,1'-biphenyl]-4-yl)oxazol-5(4H)-one (C2); yield 83%, (Z)-4-((1H-imidazol-2-yl)methylene)-2-(naphthalen-2-yl)oxazol-5(4H)-one (C3); yield 78%.

General procedure for synthesis of compounds (1-3)

1 equivalent of each of the oxazolones C(1-3), is boiled with 1.325 equivalent of Na₂CO₃ solution (30 ml/mmol) until completely dissolved (monitored by TLC for completion of reaction). The solution is mixed with 1.648 equivalent of glacial acetic acid.

Dry the solvents under vacuum when the reaction is completed to obtain the product.

(Z)-2-((E)-3-(4-hydroxyphenyl)acrylamido)-3-(1H-imidazol-2-yl)acrylic acid (1); The product is yellowish white powder and it was obtained in 85% yield, m.p. 200°C. 1H NMR (400 MHz, DMSO-d₆) δ 12.88 – 12.01 (m, 2H), 9.94 (s, 1H), 7.83 (s, 1H), 7.50 (d, J = 8.2 Hz, 2H), 7.44 (s, 1H), 7.42 (s, 2H), 6.82 (d, J = 8.4 Hz, 2H), 6.67 (d, J = 15.8 Hz, 1H); LC-MS (ESI), RT = 2.4 min, m/z 300 [M + H]⁺. Elemental analysis; Calculated for C₁₅H₁₃N₃O₄ : C, 60.2%; H, 4.38%; N, 14.04%; Found: C, 60.39%; H, 4.61%; N, 14.29%.

(Z)-2-([1,1'-biphenyl]-4-carboxamido)-3-(1H-imidazol-2-yl)acrylic acid (2); The product is slightly yellowish white powder and it was obtained in 80% yield, m.p. >230°C. 1H NMR (400 MHz, DMSO-d₆) δ 12.49 (s, 2H), 10.93 (s, 1H), 8.08 (d, J = 8.0 Hz, 2H), 7.90 – 7.84 (m, 3H), 7.78 (d, J = 7.7 Hz, 2H), 7.53 (t, J = 7.5 Hz, 2H), 7.47 – 7.41 (m, 2H), 6.92 (s, 1H); LC-MS (ESI), RT = 2.7 min, m/z 333 [M + H]⁺. Elemental analysis; Calculated for C₁₉H₁₅N₃O₃ : C, 68.46%; H, 4.54%; N, 12.61%; Found: C, 68.32%; H, 4.67%; N, 12.89%.

(Z)-2-(2-naphthamido)-3-(1H-imidazol-2-yl)acrylic acid (3); The product is white powder and it was obtained in 84% yield, m.p. 197°C. 1H NMR (400 MHz, DMSO-d₆) δ 12.53 (s, 2H), 10.93 (s, 1H), 8.64 (s, 1H), 8.13 (d, J = 7.9 Hz, 1H), 8.11 – 7.96 (m, 3H), 7.88 (s, 1H), 7.66 (dp, J = 12.9, 6.7, 6.1 Hz, 2H), 7.46 (s, 1H), 7.00 (s, 1H); LC-MS (ESI), RT = 2.6 min, m/z 308 [M + H]⁺. Elemental analysis; Calculated for C₁₇H₁₃N₃O₃ : C, 66.44%; H, 4.26%; N, 13.67%; Found: C, 66.72%; H, 4.53%; N, 13.8%.

General procedure for synthesis of compounds (4-6): Dissolve 2 equivalents of ethanolamine in 8 ml/mmol ethanol and stir for 5 minutes. Add 1 equivalent of oxazolone C(1-3) to the reaction mixture and stir at room temperature overnight. Filter off the precipitate formed and leave to dry.

(Z)-N-(2-hydroxyethyl)-2-((E)-3-(4-hydroxyphenyl)acrylamido)-3-(1H-imidazol-2-yl)acrylamide (4); The product is slightly yellowish white powder and it was obtained in 74% yield, m.p. 184°C. 1H NMR (400 MHz, DMSO-d₆) δ 12.18 (s, 1H), 10.21 (s, 1H), 7.83 (m, J = 12 Hz, 2H), 7.51 (d, J = 7.9 Hz, 2H), 7.43 (d, J = 15.7 Hz, 1H), 7.33 (s, 1H), 6.83 (d, J = 8.1 Hz, 2H), 6.66 (d, J = 16.6 Hz, 2H), 4.59 (s, 1H), 3.45 (m, 2H), 3.25 – 3.19 (m, 2H); LC-MS (ESI), RT = 2.6 min, m/z 342.9 [M + H]⁺. Elemental analysis; Calculated for C₁₇H₁₈N₄O₄ : C,

59.64%; H, 5.3%; N, 16.37%; Found: C, 59.9%; H, 5.42%; N, 16.63%.

(Z)-N-(3-((2-hydroxyethyl)amino)-1-(1H-imidazol-2-yl)-3-oxoprop-1-en-2-yl)-[1,1'-biphenyl]-4-carboxamide (5); The product is white powder and it was obtained in 79% yield, m.p. 210°C. 1H NMR (400 MHz, DMSO-d₆) δ 12.42 (s, 1H), 11.29 (s, 1H), 8.10 (d, J = 7.7 Hz, 2H), 7.95 (d, J = 7.3 Hz, 1H), 7.88 (d, J = 7.5 Hz, 3H), 7.78 (d, J = 7.6 Hz, 2H), 7.53 (t, J = 7.5 Hz, 2H), 7.45 (d, J = 7.2 Hz, 1H), 7.37 (s, 1H), 6.57 (s, 1H), 4.60 (s, 1H), 3.48 (s, 2H), 3.25 (d, J = 6.3 Hz, 2H). LC-MS (ESI), m/z 376.15 [M + H]⁺. Elemental analysis; Calculated for C₂₁H₂₀N₄O₃ : C, 67.01%; H, 5.36%; N, 14.88%; Found: C, 67.23%; H, 5.44%; N, 15.19%.

(Z)-N-(3-((2-hydroxyethyl)amino)-1-(1H-imidazol-2-yl)-3-oxoprop-1-en-2-yl)-2-naphthamide (6); The product is white powder and it was obtained in 80% yield, m.p. 228°C. 1H NMR (400 MHz, DMSO-d₆) δ 12.42 (s, 1H), 11.41 (s, 1H), 8.65 (s, 1H), 8.07 (dtd, J = 21.4, 16.9, 13.7, 6.3 Hz, 5H), 7.91 (s, 1H), 7.66 (p, J = 6.6 Hz, 2H), 7.39 (s, 1H), 6.60 (s, 1H), 4.66 – 4.56 (m, 1H), 3.50 (q, J = 6.1 Hz, 2H), 3.26 (q, J = 6.2 Hz, 2H); LC-MS (ESI), RT = 2.9 min, m/z 350.9 [M + H]⁺. Elemental analysis; Calculated for C₁₉H₁₈N₄O₃ : C, 65.13%; H, 5.18%; N, 15.99%; Found: C, 65.34%; H, 5.41%; N, 16.23%.

General procedure for synthesis of compounds (7-9)

Dissolve 1 equivalent of oxazolones C(1-3) in ethanol completely then add 2 equivalents of hydrazine hydrate solution dropwise and monitor by TLC. The precipitate is filtered off and dried.

(E)-N-((Z)-3-hydrazinyl-1-(1H-imidazol-2-yl)-3-oxoprop-1-en-2-yl)-3-(4-hydroxyphenyl)acrylamide (7); The product is slightly yellowish white powder and it was obtained in 71% yield, m.p. 205°C. 1H NMR (400 MHz, DMSO-d₆) δ 12.35 (s, 1H), 10.17 (s, 1H), 9.23 (s, 1H), 7.80 (s, 1H), 7.49 (d, J = 7.9 Hz, 2H), 7.40 (d, J = 15.8 Hz, 2H), 7.31 (s, 1H), 7.03 (s, 1H), 6.82 (d, J = 8.0 Hz, 1H), 6.63 (d, J = 16.8 Hz, 1H), 4.28 (s, 2H); LC-MS (ESI), RT = 2.6 min, m/z 313.9 [M + H]⁺. Elemental analysis; Calculated for C₁₅H₁₅N₅O₃ : C, 57.5%; H, 4.83%; N, 22.35%; Found: C, 57.32%; H, 5.09%; N, 22.17%.

(Z)-N-(3-hydrazinyl-1-(1H-imidazol-2-yl)-3-oxoprop-1-en-2-yl)-[1,1'-biphenyl]-4-carboxamide (8); The product is white powder and it was obtained in 69% yield, m.p. 191°C. 1H NMR (400 MHz, DMSO-d₆) δ 12.46 (s, 1H), 11.35 – 11.28 (m, 1H), 9.33 (s, 1H), 8.09 (d, J = 7.8 Hz, 2H), 7.87 (d, J = 7.2 Hz, 3H), 7.78 (d, J = 7.6 Hz, 2H), 7.52 (t, J = 7.5 Hz,

2H), 7.45 (d, $J = 7.3$ Hz, 1H), 7.35 (s, 1H), 6.50 (s, 1H), 4.32 (s, 2H). LC-MS (ESI), m/z 347.14 [M + H]⁺. Elemental analysis; Calculated for C₁₉H₁₇N₅O₂: C, 65.69%; H, 4.93%; N, 20.16%; Found: C, 65.78%; H, 5.14%; N, 20.42%.

(Z)-N-(3-hydrazinyl-1-(1H-imidazol-2-yl)-3-oxoprop-1-en-2-yl)-2-naphthamide (9); The product is white powder and it was obtained in 72% yield, m.p. 200°C. ¹H NMR (400 MHz, DMSO) δ 12.35 (s, 1H), 11.40 (s, 1H), 9.35 (s, 1H), 8.64 (s, 1H), 8.13 (d, $J = 8.2$ Hz, 1H), 8.05 (d, $J = 12.7$ Hz, 2H), 7.90 (s, 1H), 7.66 (s, 2H), 7.46 (s, 1H), 7.38 (s, 1H), 6.53 (s, 1H), 4.35 (s, 2H). LC-MS (ESI), m/z 321.12 [M + H]⁺. Elemental analysis; Calculated for C₁₇H₁₅N₅O₂: C, 63.54%; H, 4.71%; N, 21.79%; Found: C, 63.7%; H, 4.88%; N, 22.06%.

2.2. Biological Screening

2.2.1. Cell Culture

Cervical cancer (HeLa), non-small cell lung cancer (NSCLC) (A549) and prostate cancer (PC-3) cell lines were obtained from Nawah Scientific Inc., (Mokatam, Cairo, Egypt). HeLa cells were maintained in RPMI media while A549 and PC3 cells were maintained in DMEM media. All media were supplemented with 100 mg/mL of streptomycin, 100 units/mL of penicillin and 10% of heat-inactivated fetal bovine serum in humidified, 5% (v/v) CO₂ atmosphere at 37 °C.

2.2.2. Cytotoxicity Assay

Cell viability was assessed by sulforhodamine B (SRB) assay. Aliquots of 100 μ L cell suspension (5x10³ cells) were in 96-well plates and incubated in complete media for 24 h. Cells were treated with another aliquot of 100 μ L media containing drugs at various concentrations ranging from (10 μ m to 100 μ m). After 72 h of drug exposure, cells were fixed by replacing media with 150 μ L of 10% TCA and incubated at 4 °C for 1 h. The TCA solution was removed, and the cells were washed 5 times with distilled water. Aliquots of 70 μ L SRB solution (0.4% w/v) were added and incubated in a dark place at room temperature for 10 min. Plates were washed 3 times with 1% acetic acid and allowed to air-dry overnight. Then, 150 μ L of tris(hydroxymethyl)aminomethane (TRIS) (10 mM) was added to dissolve protein-bound SRB stain; the absorbance was measured at 540 nm using a BMG LABTECH®- FLUOstar Omega microplate reader (Ortenberg, Germany) [22, 23].

2.3. Molecular Modeling

2.3.1. Ligand and Protein Preparation

The designed compounds were drawn as 2D structures and converted to 3D structures and prepared for further modeling studies using the Schrödinger suite LigPrep tool. The ligand preparation parameters were as follows; force field: OPLS3, generate ionization states using Epik ionizer at pH 7 +/- 2, add metal binding sites, include original state, generate tautomers, retain specific chiralities and generate 3 per ligand. The PDB structures for JMJD3 co-crystallized with the inhibitor GSK-J1 (PDB ID: 4ASK) was downloaded from the Protein Data Bank [13]. The protein structure was then prepared using the Schrödinger suite protein preparation wizard. The following parameters were used for preprocessing; assign hydrogen bond orders, use CCD database, add hydrogens, create zero-order bonds to metals, create disulfide bonds, delete waters beyond 5 Å from het groups and generate het states using Epik at pH 7 +/- 2. The following parameters were used for refinement; hydrogen bond assignment using sample water orientations and PROPKA pH 7, remove waters with less than 5 hydrogen bonds to non-waters and perform restrained minimization by converging heavy atoms by RMSD 0.3 Å using OPLS3 force field.

2.3.2. Grid Generation and Molecular Docking

Prior to molecular docking, a docking grid was generated for the JMJD3 protein using the prepared protein structure. The grid was generated using the Schrödinger suite receptor grid preparation module using default settings. Metal and metal coordination constraints were generated by selecting the cobalt ion in the crystal structure. The generated grid and prepared ligands were then used for molecular docking using Glide [24]. Default docking settings were used for the docking run with metal and metal coordination constraints. Three output poses were generated for each ligand. The docking protocol was validated by re-docking of the co-crystallized ligand where the RMSD value was calculated to be 0.03 Å.

3. Results and Discussion

3.1. Rationale and Design of selective KDM6 inhibitors

The design idea for the proposed imidazole-based KDM6 inhibitors was inspired by structural determinants of previously reported inhibitors of KDM6 with introduced modifications to explore the

possible medicinal chemistry space of such inhibitors [13, 17-19]. Such inhibitors act through a competitive mechanism with the co-factor α -ketoglutaric acid [13]. This competition is enhanced by a carboxylic acid group which occupies the basic side pocket of the KDM6 enzyme and mimics its α -ketoglutaric acid congener. The main structural determinant critical for inhibition is a metal chelating group. This group binds to the ferrous ion co-factor at the heart of the active site and inhibits enzyme activity. The absence of such group abolishes compound activity. Finally, for KDM6 selectivity, the inhibitor should contain a hydrophobic aromatic extension to occupy a hydrophobic cleft formed by Pro1388 and Arg1246 [13].

The proposed compounds contain the main structural determinants for KDM6 inhibition and selectivity. Our proposal is to introduce a novel moiety that could replace the ionic interaction of the conventional carboxylic acid group. The imidazole ring plays this role by forming an unprecedented π - π interaction with Tyr1379, which anchors the compound to the entrance of the basic pocket previously occupied by α -ketoglutaric acid. The imidazole ring is functionalized with different metal-chelating groups that are able to bind the active site ferrous ion and achieve KDM6 inhibition. Different metal chelating groups were introduced such as carboxylic acid, hydrazide and ethanolamine tail. To achieve KDM6 selectivity, different bulky aromatic substituents are introduced. Design approach of the proposed KDM6 inhibitors is discussed in figure 1. Table 1 in supplementary information contains the structures of the synthesized compounds.

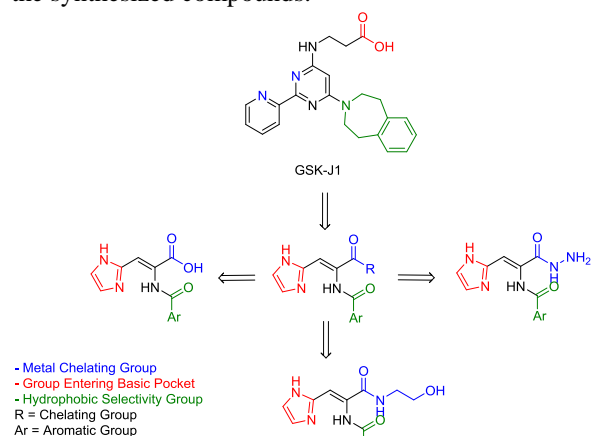
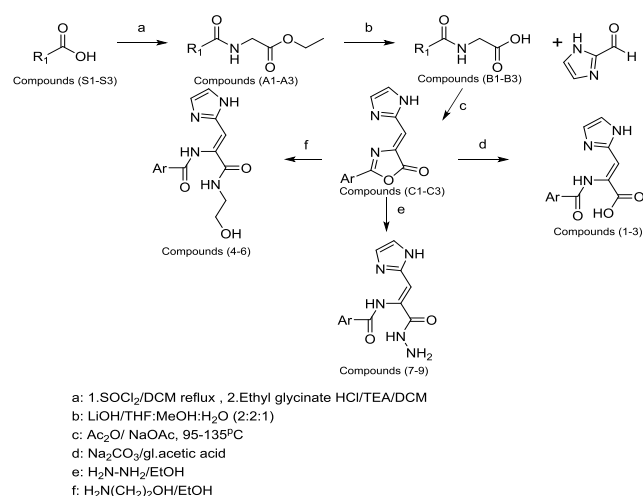


Figure 1: Design approach of the proposed compounds compared to the structural features of GSK-J1.

3.2. Synthesis of Designed Compounds

The rational design approach yielded 9 compounds that were synthesized for biological testing. Chemical synthesis started by an amide coupling step of ethyl glycinate and various carboxylic acids. This reaction yielded ethyl N-acyl glycinate derivatives. Hydrolysis of the ester yielded N-acyl glycinate which were then reacted with imidazole-2-carbaldehyde in an Erlenmeyer azlactone synthesis procedure. The formed azlactones were then cleaved using either ethanolamine, hydrazine hydrate or sodium carbonate to yield the corresponding ethanolamine derivatives, hydrazides and carboxylic acids respectively. Details of the chemical synthesis and used reagents is shown in scheme 1.



Scheme 1: General steps for the synthesis of the target compounds.

3.3. Inhibition of KDM6-Expressing Cancer Cell Lines

The designed compounds were synthesized and tested against cancer cell lines to confirm their anti-cancer activity. All the synthesized compounds were tested against KDM6-expressing cancer cell lines (HeLa). Selected cell lines are pancreatic cancer (PC-3), NSCLC (A549) and cervical cancer. All cell lines used for the assay were previously tested against GSK-J4 and were found to be sensitive to the KDM6 inhibitor [14-16]. Of the tested compounds, compound 6 was able to achieve more than 50% inhibition against HeLa and A549 cell lines at 100 μM concentration (50.4980 % and 50.4699 % respectively). These results indicate that compound 6 is in fact able to achieve inhibition of KDM6-expressing cell lines. Percentage inhibition of cancer

cell lines of the synthesized compounds is shown in table 2. It is noted that the A549 showed the highest sensitivity to the tested compounds while PC-3 was the least sensitive.

3.4. Compound 6 Binds to KDM6 through a Metal-Chelating Mechanism

To better understand the binding mechanism and confirm the design hypothesis, we performed molecular docking studies of the synthesized compounds against the KDM6 isozyme JMJD3 (Jumonji-Containing Demethylase 3) (PDB ID: 4ASK). The results indicate that the synthesized compounds bind to JMJD3 through a metal-chelating interaction. This metal coordination is achieved through one of the three metal chelating group, with an occasional contribution of the amide carbonyl belonging to the hydrophobic amide fragment with the active site metal. This moiety inserts itself in the hydrophobic Pro1388-Arg1246 cleft. The docking pose of compound 6 showed that the imidazole ring was able to achieve a π - π stacking interaction with the side chain of Tyr1379 as designed. This interaction replaces the conventional carboxylic acid charge-charge interaction with Lys1381. Furthermore, the imidazole ring is able to form a hydrogen bonding interaction with the side chain of Asn1400 in the basic pocket. Regarding the necessary metal coordination, this compound is able to coordinate the active site cobalt ion. Cobalt is found in the crystal structure instead of the native ferrous ion as it was used in the crystallization experiment by Kruidenier *et al.* This crucial interaction is achieved through the carbonyl oxygen of the hydrophobic fragment amide group and the amide nitrogen and oxygen atoms of the ethanolamine tail which approach the cobalt ion at 2.47 Å, 2.02 Å and 1.86 Å respectively. The presence of a tridentate coordination complex with the ligand replaces the coordinating water molecule found in the crystal structure of GSK-J1 with JMJD3 [13]. An extra hydrogen bond of compound 6 with the active site of JMJD3 is found between the nitrogen of the ethanolamine tail and the side chain of Glu1392, one of the catalytic residues. This extra interaction further anchors the compound to the catalytic site of JMJD3, giving compound 6 superior binding compared to the other compounds (figure 2).

3.5. Effect of lipophilicity on compounds' activity:

To better understand the activity among the tested compounds, we correlated the percentage inhibition with the CLogP of the compound and the compound structure. The importance of this correlation is that the partition coefficient plays a critical role in passive diffusion of the compound through the cell membrane. This leads to increased intracellular

accumulation of the compound and therefore a more prominent activity [25]. Calculated LogP values from ChemDraw were used to assess this factor as an important determinant of cellular activity. The two most active compounds, compound 8 and compound 6, show positive CLogP values (table 2). On the other hand, compound 5 shows lower activity despite having a higher CLogP value. This could be due to the presence of two bulky group (ethanolamine and biphenyl) when compared to the less bulky compound 6 bearing an ethanolamine and a naphthyl group. The superior activity of compound 6 is also correlated to the strong tridentate metal chelation interaction and the reasonable size of its naphthyl group being able to fit inside the Pro1388-Arg1246 cleft

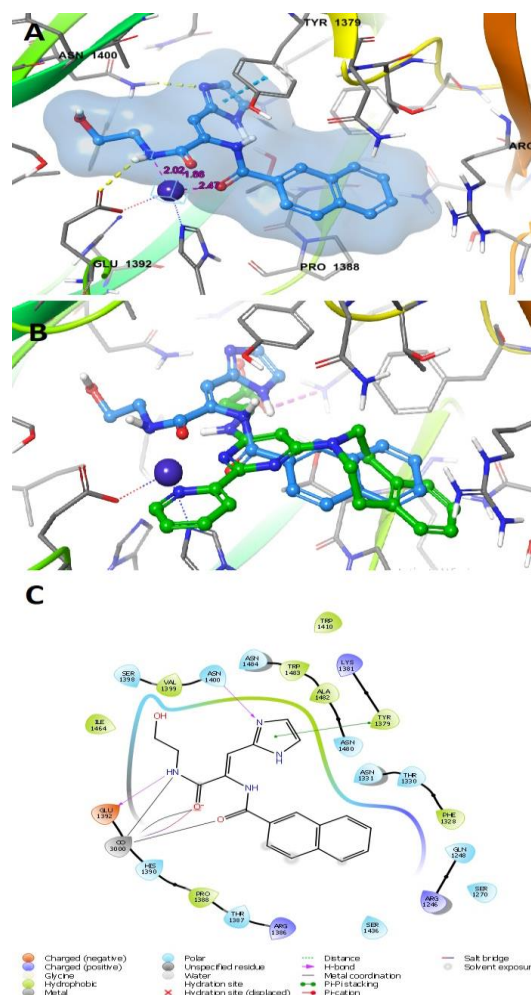


Figure 2: (A) Binding mode of compound 6 (cyan) to the active site of JMJD3. (B) Overlay of compound 6 (cyan) and GSK-J1 (green) in the binding site of JMJD3. (C) A 2D interaction diagram of compound 6 with the residues of the JMJD3 active site.

Table 1: Summary of the structures of the synthesized compounds and intermediates.

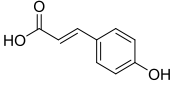
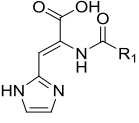
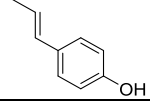
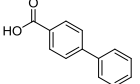
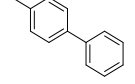
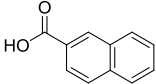
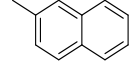
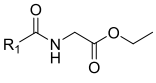
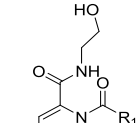
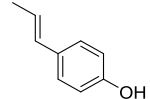
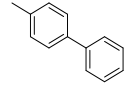
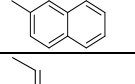
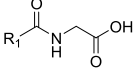
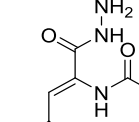
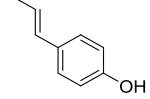
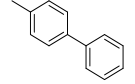
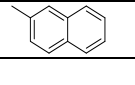
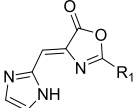




	S1			1
	S2			2
	S3			3
	A1			4
	A2			5
	A3			6
	B1			7
	B2			8
	B3			9
	C1			
	C2			
	C3			

Table 2: Percentage inhibition of cancer cell lines of the synthesized compounds and ClogP.

Compound ID	Percentage Inhibition at 100 μ M			CLogP*
	HeLa	PC-3	A549	
1	10.5850 \pm 1.4606 %	14.8168 \pm 0.4619 %	29.4212 \pm 1.8718 %	-1.9886
2	21.7980 \pm 3.1077 %	9.5366 \pm 1.7723 %	30.2204 \pm 1.2309 %	-0.2760
3	24.5910 \pm 2.7359 %	23.1950 \pm 0.4293 %	38.7599 \pm 3.2649 %	-0.9900
4	24.7940 \pm 1.8175 %	17.8071 \pm 1.1675 %	33.7539 \pm 2.7240 %	-0.0206
5	4.1160 \pm 1.0027 %	2.1834 \pm 0.9138 %	38.2388 \pm 1.6226 %	1.6920
6	50.4980 \pm 1.9962 %	10.7759 \pm 1.6204 %	50.4699 \pm 1.7334 %	0.9780
7	18.3020 \pm 0.6881 %	2.1834 \pm 0.4193 %	12.9924 \pm 0.7067 %	-0.3566
8	43.3320 \pm 0.6564 %	12.4050 \pm 2.5470 %	40.3265 \pm 1.3469 %	1.3560
9	10.3520 \pm 0.2865 %	1.6659 \pm 0.5840 %	39.2271 \pm 0.7701 %	0.6420

*ClogP is calculated using ChemDraw.

4. Conclusion

In this work, we introduced a novel series of KDM6 inhibitors through rationale and computational drug design techniques. The new compounds rely on an imidazole moiety that replaces the conventional

carboxylic acid group in the native co-factor and previously reported compounds via a π - π stacking interaction. The imidazole ring is functionalized with different metal chelating groups to achieve the crucial metal coordination interaction. A hydrophobic

fragment is also present to achieve selectivity towards KDM6. The designed compounds were synthesized and tested against KDM6-expressing cell lines where compound 6 showed the most activity. *In silico*, compound 6 demonstrated a tridentate metal coordination in a docking experiment. The activities of the tested compounds were found to correlate to the structure of the compound and the polarity represented in CLogP. This series of compounds represents a new starting point for exploring KDM6 inhibitors that do not rely on a carboxylic acid moiety. In future work, we aim to optimize the compound activities and physicochemical characteristics to achieve higher potency.

5. Acknowledgment

This work was supported by Ain Shams University Research Grants. We would like to thank Dr. Abdelsattar Omar at the Department of Pharmaceutical Chemistry, King Abdulaziz University, for providing us with the necessary molecular modelling software.

6. Conflicts of interest

The authors declare no conflict of interest.

7. Formatting of funding sources

This project was funded by Ain Shams University Research Grants.

8. References

- [1] N. Ahuja, A.R. Sharma, S.B. Baylin, Epigenetic Therapeutics: A New Weapon in the War Against Cancer, *Annu Rev Med* 67 (2016) 73-89.
- [2] A.M. El-Araby, A.A. Fouad, A.M. Hanbal, S.M. Abdelwahab, O.M. Qassem, M.E. El-Araby, Epigenetic Pathways of Oncogenic Viruses: Therapeutic Promises, *Arch Pharm (Weinheim)* 349(2) (2016) 73-90.
- [3] A. Berson, R. Nativio, S.L. Berger, N.M. Bonini, Epigenetic Regulation in Neurodegenerative Diseases, *Trends Neurosci* 41(9) (2018) 587-598.
- [4] S. Sharma, T.K. Kelly, P.A. Jones, Epigenetics in cancer, *Carcinogenesis* 31(1) (2010) 27-36.
- [5] A.E.A. Surace, C.M. Hedrich, The Role of Epigenetics in Autoimmune/Inflammatory Disease, *Front Immunol* 10 (2019) 1525.
- [6] R.A. Copeland, Epigenetic Medicinal Chemistry, *ACS Med Chem Lett* 7(2) (2016) 124-7.
- [7] A. Roberti, A.F. Valdes, R. Torrecillas, M.F. Fraga, A.F. Fernandez, Epigenetics in cancer therapy and nanomedicine, *Clin Epigenetics* 11(1) (2019) 81.
- [8] R.J. Klose, Y. Zhang, Regulation of histone methylation by demethylation and demethylation, *Nat Rev Mol Cell Biol* 8(4) (2007) 307-18.
- [9] T. Sengoku, S. Yokoyama, Structural basis for histone H3 Lys 27 demethylation by UTX/KDM6A, *Genes Dev* 25(21) (2011) 2266-77.
- [10] J. Van der Meulen, F. Speleman, P. Van Vlierberghe, The H3K27me3 demethylase UTX in normal development and disease, *Epigenetics* 9(5) (2014) 658-668.
- [11] J. Van der Meulen, F. Speleman, P. Van Vlierberghe, The H3K27me3 demethylase UTX in normal development and disease, *Epigenetics* 9(5) (2014) 658-68.
- [12] J.S. Burchfield, Q. Li, H.Y. Wang, R.F. Wang, JMJD3 as an epigenetic regulator in development and disease, *Int J Biochem Cell Biol* 67 (2015) 148-57.
- [13] L. Kruidenier, C.W. Chung, Z. Cheng, J. Liddle, K. Che, G. Joberty, M. Bantscheff, C. Bountra, A. Bridges, H. Diallo, D. Eberhard, S. Hutchinson, E. Jones, R. Katso, M. Leveridge, P.K. Mander, J. Mosley, C. Ramirez-Molina, P. Rowland, C.J. Schofield, R.J. Sheppard, J.E. Smith, C. Swales, R. Tanner, P. Thomas, A. Tumber, G. Drewes, U. Oppermann, D.J. Patel, K. Lee, D.M. Wilson, A selective jumonji H3K27 demethylase inhibitor modulates the proinflammatory macrophage response, *Nature* 488(7411) (2012) 404-8.
- [14] M. Daures, M. Idrissou, G. Judes, K. Rifai, F. Penault-Llorca, Y.J. Bignon, L. Guy, D. Bernard-Gallon, A new metabolic gene signature in prostate cancer regulated by JMJD3 and EZH2, *Oncotarget* 9(34) (2018) 23413-23425.
- [15] M.E. McLaughlin-Drubin, C.P. Crum, K. Munger, Human papillomavirus E7 oncoprotein induces KDM6A and KDM6B histone demethylase expression and causes epigenetic reprogramming, *Proc Natl Acad Sci U S A* 108(5) (2011) 2130-5.
- [16] H. Watarai, M. Okada, K. Kuramoto, H. Takeda, H. Sakaki, S. Suzuki, S. Seino, H. Oizumi, M. Sadahiro, C. Kitanaka, Impact of H3K27 Demethylase Inhibitor GSKJ4 on NSCLC Cells Alone and in Combination with Metformin, *Anticancer Res* 36(11) (2016) 6083-6092.
- [17] A. Giordano, G. Forte, S. Terracciano, A. Russo, M. Sala, M.C. Scala, C. Johansson, U. Oppermann, R. Riccio, I. Bruno, S. Di Micco, Identification of the 2-Benzoxazol-2-yl-phenol Scaffold as New Hit for JMJD3 Inhibition, *ACS Med Chem Lett* 10(4) (2019) 601-605.
- [18] A. Giordano, F. Del Gaudio, C. Johansson, R. Riccio, U. Oppermann, S. Di Micco, Virtual Fragment Screening Identification of a Quinoline-5,8-dicarboxylic Acid Derivative as a Selective JMJD3 Inhibitor, *ChemMedChem* 13(12) (2018) 1160-1164.
- [19] C. Esposito, L. Wiedmer, A. Caflisch, In Silico Identification of JMJD3 Demethylase Inhibitors, *J Chem Inf Model* 58(10) (2018) 2151-2163.
- [20] M.E. El-Araby, A.M. Omar, M.T. Khayat, H.A. Assiri, A.M. Al-Abd, Molecular Mimics of Classic P-Glycoprotein Inhibitors as Multidrug Resistance Suppressors and Their Synergistic Effect on Paclitaxel, *PLoS One* 12(1) (2017) e0168938.
- [21] K. Fendler, B. Hager, H.J.M.f.C.-C.M. Falk, The thermal diastereomerization of the tryptophane-derived green fluorescent protein chromophore, *138(9)* (2007) 859-862.
- [22] P. Skehan, R. Storeng, D. Scudiero, A. Monks, J. McMahon, D. Vistica, J.T. Warren, H. Bokesch, S. Kenney, M.R. Boyd, New colorimetric cytotoxicity assay for anticancer-drug screening, *J Natl Cancer Inst* 82(13) (1990) 1107-12.
- [23] R.M. Allam, A.M. Al-Abd, A. Khedr, O.A. Sharaf, S.M. Nofal, A.E. Khalifa, H.A. Mosli, A.B. Abdel-Naim, Fingolimod interrupts the cross talk between estrogen metabolism and sphingolipid metabolism within prostate cancer cells, *Toxicol Lett* 291 (2018) 77-85.
- [24] R.A. Friesner, R.B. Murphy, M.P. Repasky, L.L. Frye, J.R. Greenwood, T.A. Halgren, P.C. Sanschagrin, D.T. Mainz, Extra precision glide: docking and scoring incorporating a model of hydrophobic enclosure for protein-ligand complexes, *J Med Chem* 49(21) (2006) 6177-96.
- [25] B.J. Bennion, N.A. Be, M.W. Mc Nerney, V. Lao, E.M. Carlson, C.A. Valdez, M.A. Malfatti, H.A. Enright, T.H. Nguyen, F.C. Lightstone, T.S. Carpenter, Predicting a Drug's Membrane Permeability: A Computational Model Validated With in Vitro Permeability Assay Data, *J Phys Chem B* 121(20) (2017) 5228-5237.